Bioactive Materials 5 (2020) 318–333

Contents lists available at ScienceDirect

Bioactive Materials

journal homepage: http://www.keaipublishing.com/biomat

In vitro degradation of pure magnesium—the synergetic influences of glucose and albumin

Wei Yan[a], Yi-Jie Lian[a], Zhi-Yuan Zhang[a], Mei-Qi Zeng[a], Zhao-Qi Zhang[a], Zheng-Zheng Yin[a], Lan-Yue Cui[a], Rong-Chang Zeng[a,b,*]

[a] Corrosion Laboratory for Light Metals, College of Material Science and Engineering, Shandong University of Science and Technology, Qingdao, 266590, China
[b] School of Materials Science and Engineering, Zhengzhou University, Zhengzhou, 450002, China

ARTICLE INFO

Keywords:
Pure magnesium
Albumin
Degradation
Glucose
Biomaterial

ABSTRACT

The biocorrosion of magnesium in the external physiological environment is still difficult to accurately evaluate the degradation behavior in vivo, particularly, in the microenvironment of the patients with hyperglycemia or diabetes. Thus, we explored the synergistic effects of glucose and protein on the biodegradation of pure magnesium, so as to have a deeper understanding the mechanism of the degradation in vivo. The surface morphology and corrosion product composition of pure magnesium were investigated using SEM, EDS, FTIR, XRD and XPS. The effect of glucose and albumin on the degradation rate of pure magnesium was investigated via electrochemical and immersion tests. The adsorption of glucose and albumin on the sample surface was observed using fluorescence microscopy. The results showed that the presence of 2 g/L glucose changed the micromorphology of corrosion products on the magnesium surface by reacting with metal cations, thus inhibiting the corrosion of pure magnesium. Protein formed a barrier layer to protect the magnesium at early stage of immersion. The chelation reaction between protein and magnesium surface might accelerate the degradation at later stage. There may be a critical glucose (albumin) content. Biodegradation of pure magnesium was inhibited at low concentrations and promoted at high concentrations. The synergistic effect of glucose and protein restrained the adsorption of aggressive chloride ions to a certain extent, and thus inhibited the degradation of pure magnesium considerably. Moreover, XPS results indicated that glucose promoted the adsorption of protein on the sample surface.

1. Introduction

Biodegradable magnesium (Mg) alloys have attracted great interest of scientists in biomedical fields due to their excellent mechanical compatibility and biocompatibility [1–6]. Compared with traditional metal materials such as titanium alloy and stainless steel, the density of magnesium and magnesium alloy (1.74–1.80 g/cm^3) is similar to that of human bone (1.75 g/cm^3), and has higher specific strength and stiffness [5,7–10]. The young's modulus of magnesium alloy (41–45 GPa) comes near to that of human ossature (40–57 GPa) [11], which can effectively alleviate the “stress shielding” effect [12]. Mg is abundant in human body and one of essential elements for many metabolic reactions, such as muscle contraction and bone metabolism. Due to the biodegradability of Mg alloys, the degradation products are soluble and non-toxic substance, which are beneficial in physiology and can effectively avoid the second operation after tissue healing [13–15]. Moreover, Mg ions, produced by the degradation of Mg alloy implants in human body, can be excreted with urine, which do not cause other complications [16]. Therefore, Mg and its alloys have a broad application prospect in the fields of screw and plate, vascular stent, plastic surgery and so on [17–24]. In vivo experiments showed that the degradation rate of magnesium-based implants is too rapid in physiological environment to meet the clinic requirements. The severe and uncontrollable biocorrosion process significantly reduced the mechanical strength of the implants, resulting in the loss of the support before the implants fully heal [25–28]. Thus, it is very important to manipulating the degradation rate of magnesium alloys and we need to have a thorough understanding of the degradation mechanism of Mg alloys [29,30]. In the physiological evaluation of biomaterials, in vivo corrosion test is quite time-consuming, while in vitro corrosion test is more convenient and

Peer review under responsibility of KeAi Communications Co., Ltd.
* Corresponding author. Corrosion Laboratory for Light Metals, College of Material Science and Engineering, Shandong University of Science and Technology, Qingdao, 266590, China.
E-mail address: rczeng@foxmail.com (R.-C. Zeng).

https://doi.org/10.1016/j.bioactmat.2020.02.015
Received 4 January 2020; Received in revised form 22 February 2020; Accepted 23 February 2020

economical in the early research. Therefore, it is necessary to study the corrosion behavior of Mg alloy in simulated body fluid in vitro [31]. However, there is a huge gap between the in vitro corrosion and in vivo degradation behavior of Mg and its alloys. We need a more simulating in vitro medium to obtain more reliable in vitro detection results [32–39]. So far, an enormous number of researches have shown that the corrosion behavior of Mg alloys depends on its chemical composition, microstructure and production process, as well as its physiological environment [40,41]. Many corrosion studies have been developed to evaluate the corrosion degradation behavior [42] of different Mg alloys (AZ31, AZ91, Mg–Ca, Mg–Zn and pure Mg) in different in vitro physiological environments (0.9 wt% sodium chloride (NaCl) solution, simulated body fluid (SBF), phosphate buffer solution (PBS) and Hank's solution) [35,43,44]. Most studies are focused on the influence of inorganic ions (including Ca^{2+}, Mg^{2+}, Cl^{-}, SO_4^{2-}, HCO_3^{-}, CO_3^{2-}, HPO_4^{2-}, $H_2PO_4^{-}$) in body fluids on the biodegradation behavior of magnesium alloys in vitro [17,43,45–47]. In contrast, the role and interactions of organic compounds (glucose, amino acids, protein, etc.) in the regulation of magnesium alloy degradation are not understood deeply [11,43,48–54].

Glucose (Glu) is a monosaccharide, a kind of polyhydroxy aldehyde. As the energy source of living cells and the intermediate product of metabolism, glucose is widely used as a medium for clinical injection of drugs to patients. The previous studies [55–58], performed by our group, have shown that glucose and its concentration have different influences on the degradation behavior of pure Mg in saline and Hank's solutions. On one hand, glucose promotes the corrosion rate of pure magnesium in saline solution. Glucose is rapidly converted into gluconic acid, which can reduce the pH value of the solution and encourage the adsorption of chloride ions on magnesium surface, thus accelerating corrosion [55]. On the other hand, the existence of glucose improves the corrosion resistance of pure Mg in Hank's solution, which is caused by the formation of calcium phosphate compound on the surface of the samples by the coordination of gluconic acid and Ca^{2+}. The effect of glucose on the degradation behavior of Mg–Ca alloy and AZ31 in saline solution was further investigated [57,58]. The results showed that the presence of glucose accelerated the corrosion kinetics of Mg-1.35Ca alloy in saline solution. The corrosion resistance of AZ31 alloy was improved in the presence of 1 g/L glucose, while aggravated in the addition of 2 and 3 g/L glucose [57,58]. It is concluded that the degradation mechanism and corrosion products of different magnesium alloys in different SBFs are diverse. Therefore, it is necessary to further explore the interaction between biodegradable magnesium and glucose in specific physiological environment. It is reported [59] that the glucose in human body is about 0.7–1.5 g/L, while in normal people it can be as high as 1.8 g/L, and in diabetics it can even reach more than 2 g/L. In addition, glucose is injected into the human body as a clinical medicine medium (5 wt%) to increase the glucose concentration in the body, so the glucose concentration we selected in this experiment is 2 g/L [56].

Protein is an organic macromolecule and the main participant of life activities. Therefore, protein plays an important role in the biodegradation of Mg alloys in human body. So far, many studies have been carried out to evaluate the effect of protein on the degradation rate of different magnesium alloys in diverse media and different conclusions have been drawn [51–53]. It is generally believed that the degradation behavior of magnesium alloy is mainly affected by protein adsorption and chelation. For one thing, protein will be adsorbed on the magnesium alloy surface as a diffusion barrier between metal surface and medium environment, which can inhibit the sorption of aggressive ions and thus reduce the corrosion rate of magnesium alloys. For another thing, the chelation between magnesium ions and amino acid molecules reduces the barrier effect of insoluble salt layer on magnesium dissolution [32]. Yamamoto et al. [43] studied the corrosion rate of fetal bovine serum (FBS) on pure Mg in NaCl and eagle's minimum essential medium (E-MEM). The results showed that the adsorption of protein and the insoluble precipitation reduces the degradation rate. Wan et al. [60] explored the corrosion mechanism of albumin on PEO coated magnesium in NaCl and PBS solutions. Liu et al. [61] deemed that the degradation rate of AZ91 in SBF was about twice that in SBF + 1 g/L albumin. Rettig et al. [62] studied the effect of albumin on electrochemical behavior of WE43 alloy in SBF. The results showed that the inhibition of albumin was owing to the formation of a sealing layer on the surface in the first few hours of exposure. Mueller et al. [63] studied the degradation behavior of magnesium alloys (pure Mg, AZ31 and LAE442) in NaCl and PBS electrolytes containing different Cl^{-} and albumin concentrations. Hou et al. [32] explored the adsorption of BSA and fibrinogen on the surface of pure magnesium in different media (Hank's and DMEM). Kim et al. [50] briefly introduced the process of protein adsorption (Vroman effect) from the perspective of kinetics. In conclusion, the reaction between magnesium alloy and protein is related to the type of magnesium alloy, reaction time and medium environment. As we all know, the basic unit of protein is amino acid. In order to better explore the effect of protein on the degradation behavior of magnesium alloy, we should first explore the effect of amino acid on the surface of magnesium alloy. Wang et al. in our group [56] studied the coupling effect of amino acid and glucose on the degradation behavior of pure magnesium in normal saline (0.9 wt% NaCl) solution. Glucose or amino acid can inhibit the degradation of pure magnesium, while glucose and amino acid can react to form Schiff base to promote the degradation of magnesium. Furthermore, Wang et al. [64] further explored the influences of isoelectric point and molecular structure of different amino acids (alanine, glutamic acid and lysine) on the degradation behavior of pure Mg in PBS and proposed the reasonable corrosion mechanism of amino acids to pure Mg. However, more systematic research is needed to discuss the reaction mechanism of protein.

The objective of the present study is to probe the synergistic effects of glucose and protein on the biodegradation of pure Mg, and to deeply explore its degradation mechanism from a new angle.

2. Experimental

2.1. Materials and chemicals

The experimental materials used for this investigation were as-cast pure magnesium with a purity of 99.97%, supplied by Guangling Magnesium Industry Science and Technology Co. Ltd. (Beijing, China). Magnesium plate is cut into small pieces of the same size (20 mm × 20 mm × 5 mm). Then the samples were polished with SiC sandpaper (grid range of #150–2500), and then cleaned with distilled water and ethanol for 5 min at room temperature, followed by drying via warm air at room temperature prior to the corrosion tests. The fluorescein disodium salt comes from Shanghai Yuanye Biotechnology Co., Ltd. The chemicals contained sodium chloride (NaCl), glucose ($C_6H_{12}O_6$) and protein (Bovine serum albumin) were purchased from Qingdao Jingke Chemical Reagent Co., Ltd., China [56].

2.2. Hydrogen evolution measurement

The solution used in the hydrogen evolution measurement is appeared in Table 1. Each group of hydrogen evolution tests contains four

Table 1
Concentration of the chemicals of the solutions for immersion tests, g/L.

Solution	NaCl	Glucose ($C_6H_{12}O_6$)	Protein (BSA)
NaCl	9.0	–	–
NaCl + Glu	9.0	2.0	–
NaCl + BSA	9.0	–	0.1
NaCl + Glu + BSA	9.0	2.0	0.1

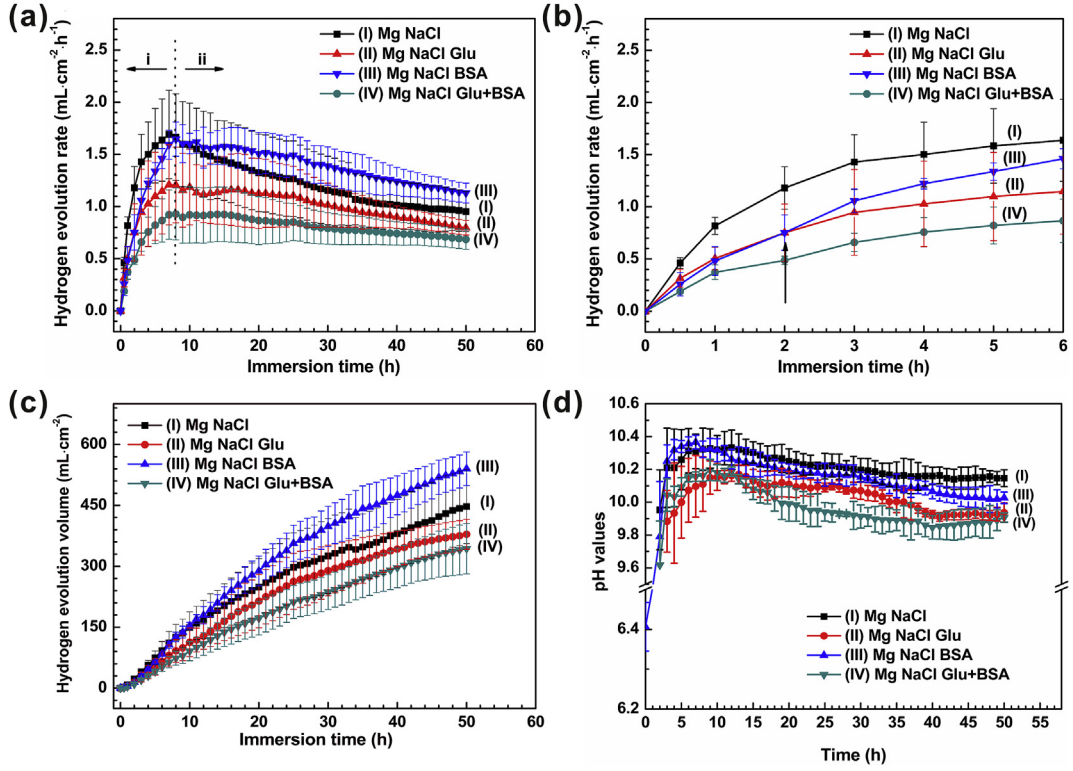

Fig. 1. Curves of (a), (b) hydrogen evolution rate (HER), (c) hydrogen evolution volume (HEV) and (d) pH values as functions of immersion time.

parallel samples. In order to avoid the influence of anions such as phosphate, sulfate and bicarbonate, we selected a simple saline solution. The BSA concentration (0.1 g/L) was selected according to the concentration in human plasma. E. Balint et al. [65] suggested that the plasma glucose content in normal subjects ranged from 4.6 to 6.1 mmol, 10 mmol/L after meals, and 15 mmol/L in hyperglycemic subjects. The hydrogen evolution measurements were carried out in a water bath at 37 ± 0.5 °C. The pure Mg samples were put into beakers containing different solutions. Furthermore, the funnel was placed on a plate with holes to make sure measure hydrogen generated by degradation of pure magnesium accurately. The effect of glucose and protein concentration on corrosion rate of Mg should be further investigated. The corresponding hydrogen evolution rate (HER, V_H) can be expressed as follows:

$$V_H = V/St \tag{11}$$

where V is the volume of hydrogen (mL); S and t are the surface area (cm^2) and soaking time (h) in saline solution, respectively.

The hydrogen volume and the pH value of the solution were taken notes at 30 min intervals for the first 10 h, and then at 60 min. The pH value was gauged by a benchtop pH meter (type PH400) [66].

2.3. Electrochemical experiment

The electrochemical behavior of pure magnesium in saline solution was investigated by electrochemical workstation (VersaSTAT 4). The cell is a standard three-electrode working system. Magnesium samples are used as working electrodes, saturated calomel electrodes (SCE) as reference electrodes, and platinum electrodes as opposite electrodes. The potentiodynamic polarization curves and Electrochemical Impedance Spectroscopy (EIS) were measured after the electrode stabilization time of 600 s. EIS measurements were carried out at frequencies of 1 kHz–10 mHz. The potentiodynamic polarization curve started from approximately −2000 to −1000 mV at a scanning rate of 2 mV/s. Each solution was tested three times in parallel. Moreover, the higher the polarization resistance (R_p), the lower the corrosion rate. R_p can be calculated by stern Geary equation:

$$R_p = \frac{\beta_a \cdot \beta_c}{2.303 i_{corr}(\beta_a + \beta_c)} \tag{12}$$

where, i_{corr} is the self-corrosion current density; β_c and β_a represent the slope of cathode and anode polarization curves, respectively [67].

2.4. Surface analysis

The surface functional groups of the samples were detected using Fourier transform infrared spectroscopy (FTIR, Nicolet380, Thermo Electron Corporation, USA). The phase composition of corrosion products was distinguished by an X-ray diffraction diffractometer (XRD, Riguta D/max 2500 PC, Japan) with a Cu Ka1 (λ = 0.15406 nm) source operated at 35 kV and 20 mA. The microstructure and surface morphology of pure Mg samples after hydrogen evolution test were characterized with field emission scanning electron microscope (FE-SEM, NOVA NANOSEM-450, USA). The chemical compositions of pure Mg surface corrosion products were probed by energy dispersive X-ray spectroscopy (EDS) and X-ray photoelectron spectroscopy (XPS, ESCALAB 250, Thermo VG Corporation, MA, USA) [56].

2.5. Fluorescent Labeling experiment

The samples with the size of 10 mm × 10 mm × 5 mm were put into 24-well plates, and then added 2 mL 0.9 wt% NaCl solution, 2 mL 0.9 wt% NaCl solution containing 2 g/L glucose, 2 mL 0.9 wt% NaCl solution containing 0.1 g/L bovine albumin, 2 mL 0.9 wt% NaCl solution containing 2 g/L glucose and 0.1 g/L bovine albumin, respectively. The next step is to put the samples in a 37 °C incubator for 0.5 h, 2 h and 24 h, then take it out and wash it three times with NaCl solution, 5 min each time, and blow it dry. Subsequently, each sample was dripped with 50 μL fluorescein isothiocyanate (FTIC); 24 orifice plates were placed in a refrigerator at 4 °C for 12 h, and then washed with

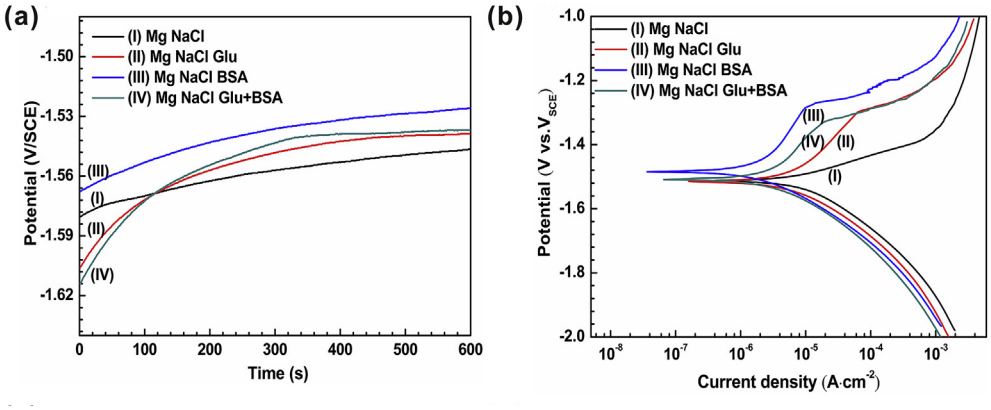

Fig. 2. The plots of (a) open circuit potential (OCP) and (b) potentiodynamic polarization; The bar graphs of (c) Potential and (d) Current density of pure Mg immersed in different saline solutions.

methanol for three times, 5 min each time. Free FTIC was washed and dried with NaCl solution for 5 min. Fluorescence microscopy (FM, Leica DM2500, Germany) was taken for photograph to detect the albumin. Similarly, sodium fluorescein is used to fluorescently label glucose [68].

3. Results

3.1. Immersion test

Fig. 1 depicts (a), (b) the hydrogen evolution rate (HER) and (c) hydrogen evolution volume (HEV) of pure Mg immersed in different saline solutions (with protein or/and glucose) at 37 ± 0.5 °C for 50 h. The curve of hydrogen evolution rate can basically characterize the change of sample's degradation rate. The samples possess a lower rate value at the initial stage of immersion test, which may be attributed to the formation of oxide film on the surface of pure Mg. At the initial immersion time of 2 h, the degradation rates of the samples are ranked as follows: NaCl solution > NaCl + Glu solution > NaCl + BSA solution > NaCl + Glu + BSA solution. During the immersion time of 2–8 h, the HER of various saline solutions increases rapidly. And it is noted that the HER in saline solution containing albumin was higher than that in glucose solution. Subsequently, the HER in NaCl + BSA solution is the highest, and the degradation rate of samples in four solutions gradually decrease. According to the curve change trend of the solution of NaCl + BSA, we could analyze that protein has a strong impact on the degradation behavior of pure magnesium through the combined action of adsorption and chelation. In the initial stage, adsorption is much faster than chelation, and the bovine albumin adsorbs rapidly, and acts as a barrier layer on the pure magnesium surface [69], resulting in the decrease of corrosion rate in the initial stage. With the increase of soaking time, chelation gradually becomes more prominent than adsorption, which leads to higher degradation rate. The HER in the solution of NaCl + Glu + BSA is the lowest owing to the synergetic effects of glucose and albumin, which formed a dense adsorption layer and inhibited the degradation of samples. Ultimately, HER remains steady owing to the consumption of Glu and BSA and the accumulation of protective films. Note that the HEV results in Fig. 1(c) correspond to the change of specimen's degradation rate.

Generally, the change of HER corresponds to the pH value of the solution. The change of solution pH during immersion time is shown in Fig. 1(d). The initial solution pH values are ranked in the following order: NaCl + BSA < NaCl + Glu + BSA < NaCl + Glu < NaCl solution. Obviously, the NaCl solution is nearly neutral. The other three solutions are weakly acidic when glucose and/or protein were added. This may be owing to the conversion of glucose into gluconic acid, and more acidic amino acid groups than basic groups in albumin. The degradation of pure Mg could increase the pH value of all specimens to a certain extent. The curve of pH value as a function of soaking time goes through three stages: rapid increase in early stage (0–4 h); the slow ascending stage; and the slightly decreasing subsequent horizontal stage. It is noteworthy that the HER in the solution of NaCl + BSA and NaCl + Glu + BSA began to decrease at 8 h and 12 h of immersion, respectively. At the immersion time of 8 h, the pH value of NaCl + BSA solution begins to decrease, and is lower than that of the NaCl solution. Ultimately, after 12 h, the pH value of NaCl + Glu + BSA solution is lower than that of NaCl + Glu solution. This may be owing to the dissolution of $Mg(OH)_2$ precipitate in the solution of NaCl + BSA to form soluble $MgCl_2$ and the continuous formation of $Mg(OH)_2$ degradation product layer in NaCl solution. The order of pH value of saline solutions changes as follows: 0.9 wt% NaCl > 0.9 wt% NaCl containing albumin > 0.9 wt% NaCl containing glucose and albumin > 0.9 wt% NaCl containing glucose. Obviously, the corresponding pH value has a prominent influence on HER.

3.2. Electrochemical experiments

The degradation behavior of pure magnesium in four different solutions is characterized by open circuit potential (OCP), potentiodynamic polarization curve and electrochemical impedance spectroscopy (EIS). As depicted in Fig. 2(a), the OCP curves of pure Mg in four different solutions rise continuously and slightly float and show a small zigzag shape in the whole test process, which means that the magnesium dissolves and gradually forms a corrosion product layer at the interface until reaching a steady state [45]. Moreover, the potential value reduces progressively in following order: NaCl + BSA solution > NaCl + Glu + BSA solution > NaCl + Glu solution > NaCl solution, which also indicates that corrosion behavior of pure magnesium in different solutions in early stage. The polarization curves (Fig. 2(b)) indicate that the sample in NaCl + BSA solution has the highest potential (E_{corr}) and the minimum self-corrosion current density (i_{corr}). It could be apparent that breakdown potential (E_b) exists in the solutions of NaCl + Glu and NaCl + BSA, and the E_b in NaCl + Glu solution was higher than that in NaCl + BSA solution. The passivation of the anode curve in NaCl + Glu solution indicates that a protective layer is formed on the surface of the sample. The parameters of polarization curves for pure magnesium in diverse solutions are enumerated in Table 2 [70]. The data indicate that the existence of BSA reduces the degradation rate in NaCl + BSA solution compared with that in NaCl solution. However, the synergetic effects of albumin and glucose slightly accelerate the degradation behavior of pure Mg in NaCl + Glu + BSA solution.

The Nyquist diagram of pure Mg immersed in four solutions (Fig. 3(c)) contains a low frequency inductive reactance arc, low frequency capacitive reactance arc and high frequency capacitive reactance arc [17]. The maximum diameters of capacitance rings of NaCl,

Table 2
Electrochemical parameters obtained from the polarization curves of pure Mg in different solutions.

Solution	E_{corr}	I_{corr}	β_a	$-\beta_c$	R_p
	(V/SCE)	(10^{-6} A cm^{-2})	(mV·decade^{-1})	(mV·decade^{-1})	(10^4 Ω cm [2])
NaCl	−1.51 ± 0.02	8.36 ± 2.43	57.23 ± 11.26	105.75 ± 8.24	0.65 ± 0.55
NaCl Glu	−1.51 ± 0.06	7.47 ± 2.57	139.87 ± 17.60	85.33 ± 9.53	1.27 ± 0.35
NaCl BSA	−1.48 ± 0.09	3.35 ± 1.29	235.19 ± 21.42	94.82 ± 11.24	2.06 ± 0.80
NaCl Glu + BSA	−1.51 ± 0.08	5.40 ± 1.31	147.5 ± 13.24	105.01 ± 9.26	2.93 ± 1.02

NaCl + Glu, NaCl + BSA, and NaCl + Glu + BSA solutions appear at the frequency of 63.096 mHz, 39.811 mHz, 31.623 mHz, and 31.623 mHz respectively. The capacitive loop immersed in NaCl solution is the smallest, while the capacitive loop immersed in NaCl + BSA solution is the largest, indicating that BSA can inhibit the degradation of magnesium. Nevertheless, the addition of glucose to a certain extent weakens the effect of protein on the corrosion resistance of pure Mg samples. This finding is somewhat different from the results of hydrogen evolution test.

In order to ulteriorly comprehend the degradation behavior of pure magnesium, the fitting data of EIS are shown in Table 3. The equivalent circuits model for pure Mg in solution NaCl is shown in Fig. 3(d) ($R(Q(R(Q(LR))))$). R_s stands for the resistance of solutions. The equivalent circuits model for pure Mg in three other solutions is shown in Fig. 3(e) ($R(Q(R(QR))(LR))$). We can see that the solution resistance increases slightly after adding glucose or protein from Table 3. The variables L and R_L, used to describe the low-frequency inductive reactance arc, represent the inductance and resistance, respectively. The existence of inductive reactance arc indicates the existence of pitting corrosion on the sample surface. It is more practical to simulate an electric double layer with a constant phase angle element (CPE) in most electrode systems due to the dispersion effect of the activation energy distribution in the space charge layer and the roughness and inhomogeneity of the electrode surface. CPE corresponds to capacitance of the system. Charge transfer resistance is expressed by R_{ct}; and higher R_{ct} value means lower degradation rate of magnesium. The R_{ct} values obtained by the arc diameter of Nyquist curve can be arranged in the following order: NaCl + BSA > NaCl + Glu + BSA > NaCl + Glu > NaCl solution. In addition, the impedance modulus |Z| at low frequency is an important factor used for characterize the corrosion resistance of the specimens

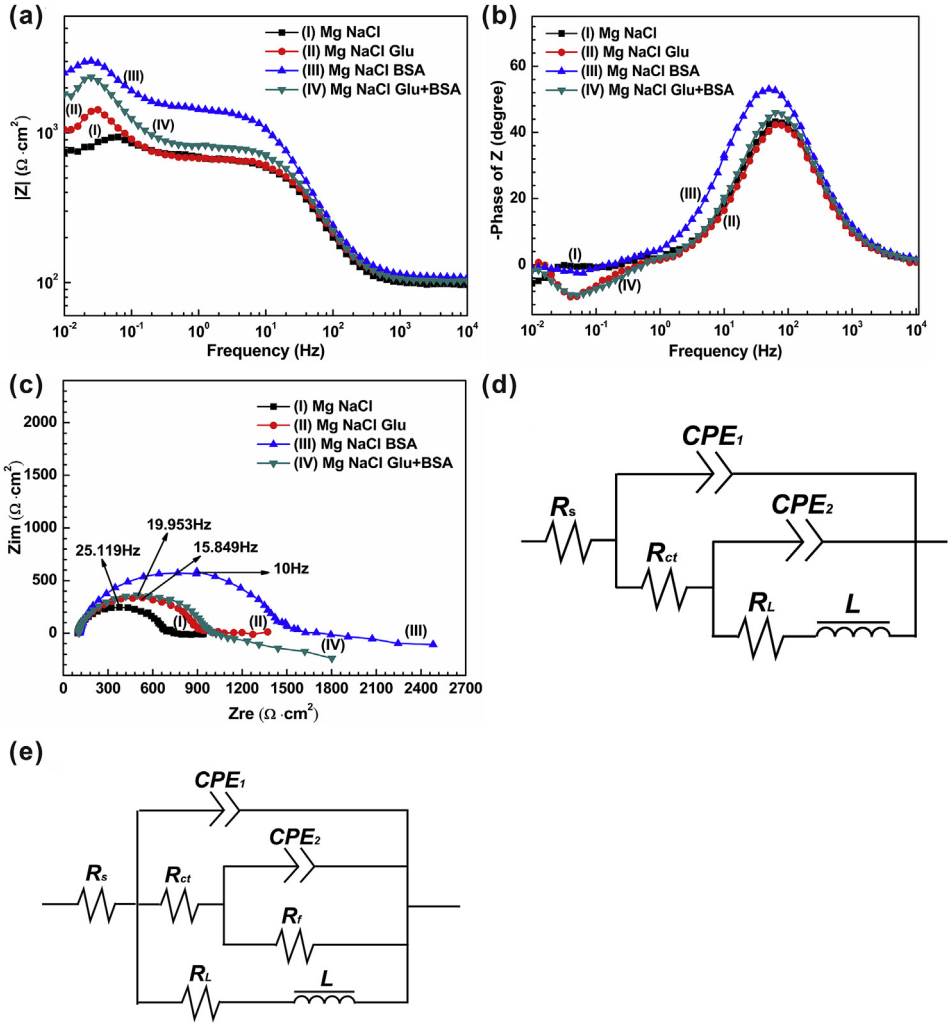

Fig. 3. The Plots of (a) Bode; (b) Bode phase curves and (c) Nyquist; and (d), (e) the equivalent circuits of the electrochemical impedance spectroscopy (EIS) spectra.

Table 3
Fitting results of the equivalent circuits of EIS curves.

Solution	R_s (Ωcm [2])	CPE_1 (10^{-5} $\Omega^{-1}s^n cm^{-2}$)	n_1	R_{ct} (10^2 Ω cm [2])	CPE_2 (10^{-3} $\Omega^{-1}s^n cm^{-2}$)	n_2	R_f (10^2 Ω cm [2])	R_L (10^2 Ω cm [2])	L (10^3 H cm^{-2})
NaCl	55.21 ± 2.34	1.85 ± 0.23	0.90 ± 0.03	3.61 ± 0.07	5.24 ± 0.56	0.20 ± 0.01	–	10 ± 0.46	5.80 ± 0.23
NaCl Glu	60.86 ± 1.42	1.49 ± 0.31	0.92 ± 0.01	4.39 ± 0.12	4.73 ± 0.42	0.25 ± 0.02	0.25 ± 0.02	0.78 ± 0.03	3.62 ± 0.16
NaCl BSA	60.09 ± 6.14	1.87 ± 0.25	0.89 ± 0.02	5.33 ± 0.21	5.06 ± 0.36	0.84 ± 0.07	2.72 ± 0.14	24.1 ± 1.36	5.38 ± 0.32
NaCl Glu+BSA	60.45 ± 4.21	1.71 ± 0.19	0.90 ± 0.02	5.13 ± 0.17	4.46 ± 0.24	0.64 ± 0.02	1.97 ± 0.11	3.71 ± 0.43	3.22 ± 0.14

(Fig. 3(a)). Generally speaking, the higher modulus |Z| represents lower degradation rate. We can perceive that the corrosion resistance outcomes of |Z| obtained from Fig. 3(a) are in accordance with Nyquist plots [7,56,64].

3.3. Surface analysis

The change of the surface composition of the sample after soaking in the albumin solution has a considerable impact on its degradation behavior. Fig. 4(a)–(d) illustrate the SEM morphologies of pure Mg after soaking in different saline solutions for 50 h. We could perceive that the sample surface immersed in solution NaCl accumulated a lot of flake corrosion products and had obvious cracks (Fig. 4(a)). Serious corrosion emerges on the samples. Some network corrosion products and a little accumulation are formed on the sample surface in NaCl + Glu solution; and a more uniform and dense corrosion product layer ($Mg(OH)_2$) is formed (Fig. 4(b)). This indicates that the existence of glucose inhibits the degradation of magnesium alloy. After adding proteins, many irregularly disperse loose clusters of white corrosion products and deep pits can be found on the whole surface, which means that the samples are seriously corroded after long-term immersion in saline solution in the presence of proteins (Fig. 4(c)). The next morphological image shows that when glucose and protein are added at the same time, a denser reticulated product layer and a more concentrated white sediment on the surface of the sample exhibit good corrosion resistance (Fig. 4(d)) [71]. This is basically consistent with the results of hydrogen evolution.

According to the corresponding EDS spectroscopic analysis (by atomic and weight percent) (Fig. 5), the degradation products are composed of C, Mg, O, N elements and a modicum Cl element, implying that the corrosion product may be primarily composed of $Mg(OH)_2$. The EDS of spectrum #1 and #2 show that there are high content of Mg and O, and low C content on the sample surface [72]. This situation indicates that the degradation products of pure magnesium immersed in NaCl solution are mainly $Mg(OH)_2$ and a small quantity of $MgCO_3$ (few CO_2 in air dissolved in saline). Compared with the former, the C content of spectrum #3 and #4 is higher. This indicates that besides $Mg(OH)_2$ and $MgCO_3$, the added glucose also participates in the interfacial reaction and is adsorbed on the sample surface. EDS spectra of #5, #6, #7 and #8 show that the surface of the sample contains not only higher C element, but also N element and a small amount of Cl element. The elevated C element implies that organic compounds (proteins and glucose) are adsorbed on the surface and lead to a thin adsorption layer (Fig. 5). The results show that the adhesion of proteins on the Mg surface promotes the adsorption of Cl^- ions and results in more serious corrosion of Mg alloys.

Fig. 6 shows the XRD patterns of pure magnesium after different immersion time (0.5 h/50 h) in different saline solutions. The predominant peaks of Mg phase are detected in all spectrums [6]. The peaks at 18° and 38° in Fig. 6(a) indicate that a small amount of magnesium hydroxide is formed on the pure magnesium surface in NaCl solution and NaCl + Glu solution after 0.5 h of immersion, while protein adsorption on the surface of the material inhibits the formation of $Mg(OH)_2$ on the surface. And there is a small amount of magnesium carbonate on the surface. From Fig. 6(b), it can be seen that the peaks at 18°, 38°, 51°, 59°, 63 °and 73° after adding glucose or protein, prove the existence of corrosion products of $Mg(OH)_2$ on the sample surface. XRD analysis shows that BSA inhibited the formation of Mg $(OH)_2$ thin films and the degradation of pure Mg [57]. Interestingly, the surface of the sample in solution NaCl Glu after 50 h of immersion represents a strong peak of magnesium phase, which may be owing to the dissolution of the corrosion product. In addition, the adsorption of glucose and protein on the pure magnesium surface can also lead to the sorption of chloride ions and the formation of other corrosion products. ($MgCl_2{\cdot}6H_2O$ and $Mg_7(CO_3)_5(OH)_4$) [58].

The chemical structure and functional groups of corrosion products

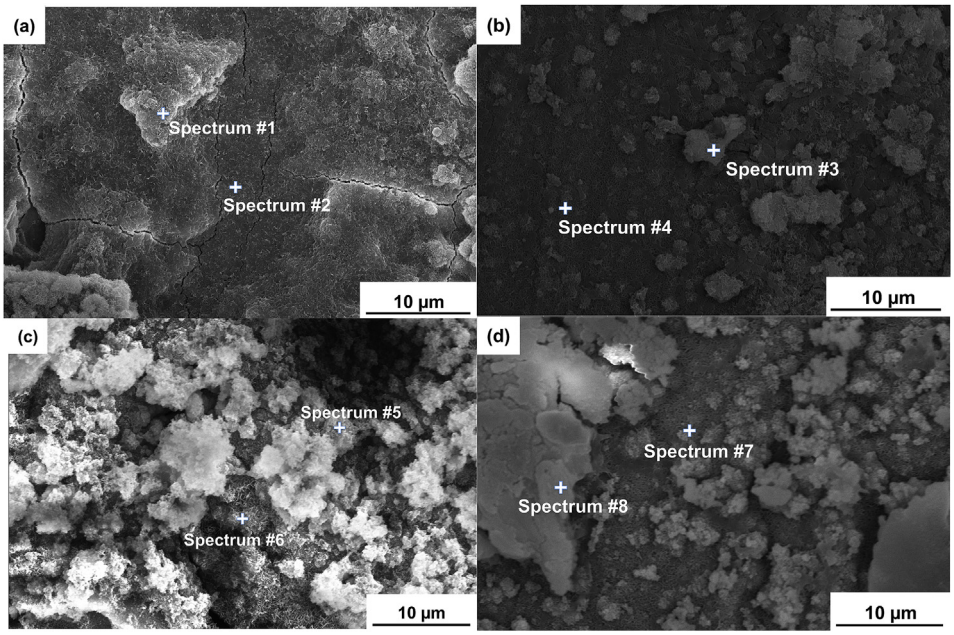

Fig. 4. SEM morphology images of the pure Mg surface after immersions of 50 h: (a) solution NaCl, (b) solution NaCl Glu, (c) solution NaCl BSA, (d) solution NaCl Glu BSA.

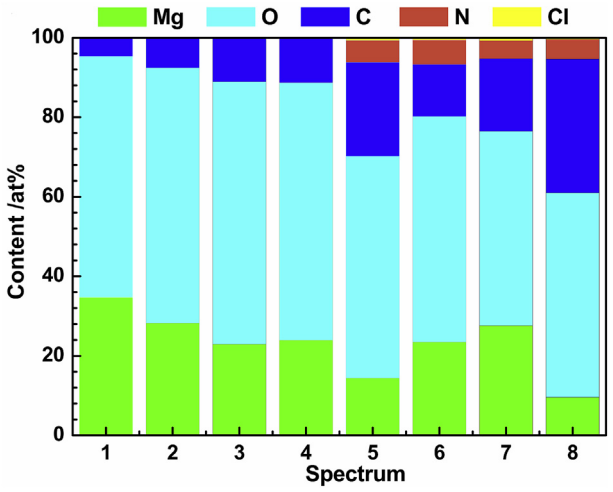

Fig. 5. The contents of various elements probed of the pure Mg surface after immersions of 50 h: #1-#2(solution NaCl), #3-#4(solution NaCl Glu), #5-#6(solution NaCl BSA), #7-#8(solution NaCl Glu BSA).

on the sample surface soaked in different solutions for 0.5 h and 50 h are analyzed by Fourier transformed infrared (FTIR) spectroscopy. As shown in Fig. 7(a), the peak at 3698 cm^{-1} is attributed to the formation of surface $Mg(OH)_2$ precipitation. The absorption bands at 3470 cm^{-1} and 3419 cm^{-1} can be ascribed to the O–H group [73]. The peak at 1658 cm^{-1} is typical for the C═O stretching of amide peptide bonds. The adsorption peak at 1441 cm^{-1} is attributed to the tensile vibration of CO_3^{2-}, which is the result of the dissolution of carbon dioxide in air into brine solution. The band around 1060 cm^{-1} can be considered to the bending vibration mode of C–H [74], which implying that the vinyl group in albumin or glucose affects the surface degradation of the sample. The Mg–O absorption band at 442 cm^{-1} states that a thin oxide film is formed on the sample surface. The above results show that the corrosion products on the sample surface after soaking for 0.5 h are mainly $Mg(OH)_2$, and after adding Glu or BSA, the residual –OH on the surface of the sample decreases. Fig. 7(b) exhibits the FTIR spectra of pure Mg after immersed in different solutions for 50 h. The absorption band at 2360 cm^{-1} could be attributed to the tensile vibration of Mg–O. The adsorption peak at 1658 cm^{-1} is attributed to the bending vibration of C═O in glucose or protein, respectively. The bands around 1062 cm^{-1} become apparent after adjunction of glucose or protein, which may be the main cause of C–O tensile vibration [51]. The absorption band of Mg–OH is observed at 564 cm^{-1}, which can be

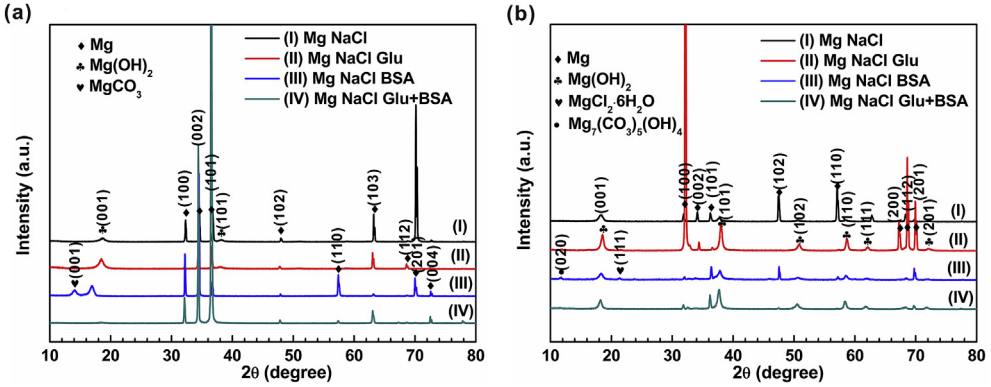

Fig. 6. XRD patterns of pure Mg immersed in four different solutions for: (a) 0.5 h; and (b) 50 h.

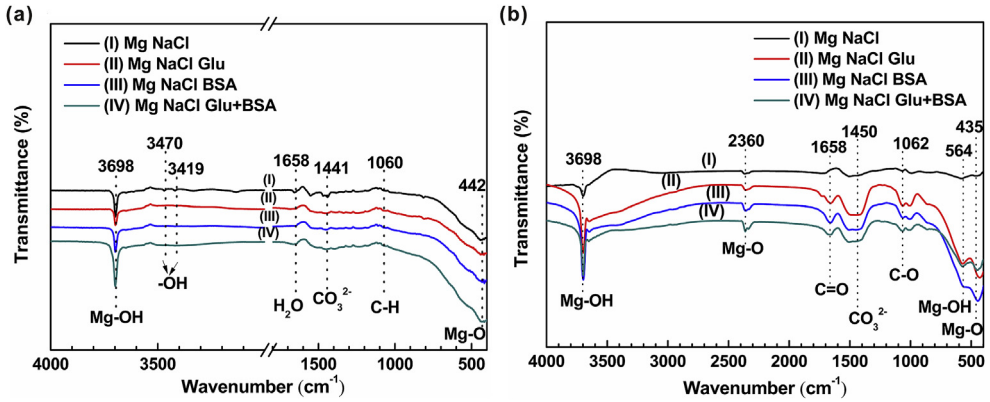

Fig. 7. Fourier transformed infrared (FTIR) spectra of the samples in four solutions after an immersion of (a) 0.5 h; and (b) 50 h.

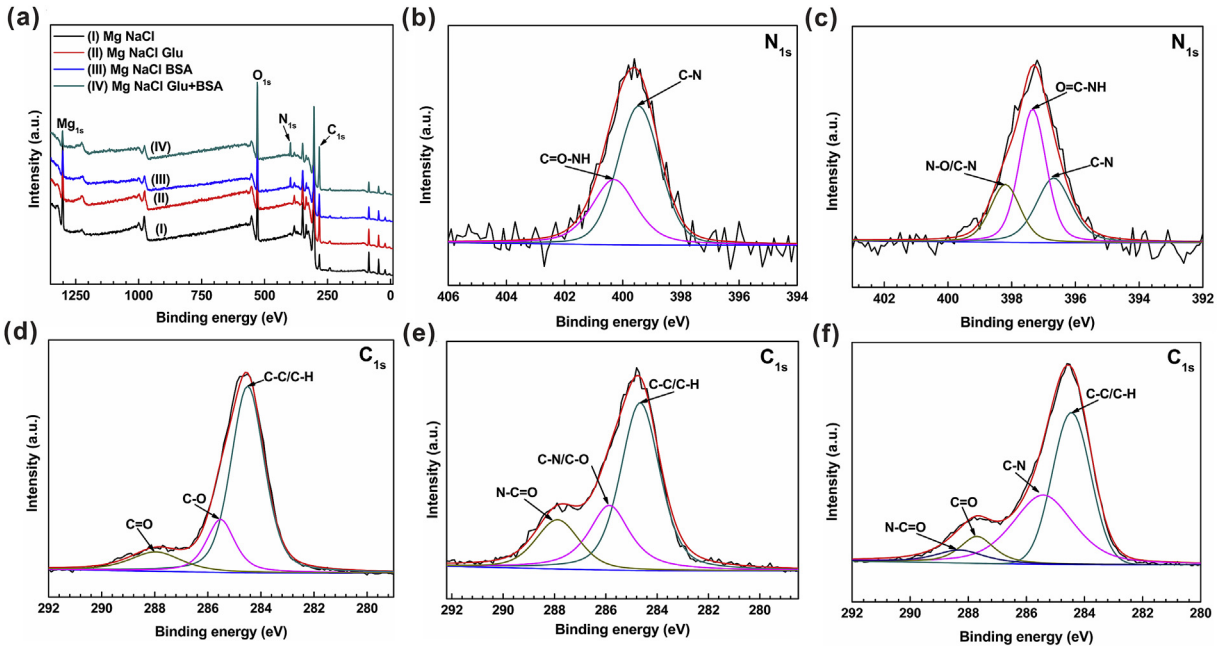

Fig. 8. XPS analysis of pure Mg immersed in four different solutions for 2 h.

attributed to the formation of surface precipitation of $Mg(OH)_2$.

XPS is applied to further study the effect of glucose or/and protein on the degradation behavior of pure Mg immersed in different saline solutions for 2 h (Fig. 8). Fig. 8(a) specifies the entire range of binding energy measurements. The results show that the corrosion products on the surface of magnesium alloy samples are mainly composed of Mg, O, N and C elements. The existence of N element confirms the existence of BSA on the sample surface. Fig. 8(d) shows the narrow spectrum of C_{1s} of pure magnesium after immersion in NaCl + Glu solution for 2 h C_{1s} spectrum can be divided into three peaks: the main peak at 284.5 eV is ascribed to C–C/C–H group; the second peak at 285.5 eV may be related to the existence of C–O group [74]; the new peak at 288.0 eV may have an bearing on the existence of C═O group. The existence of C–C/C–H group and C–O group indicates that glucose is adsorbed on the surface of pure magnesium rapidly. The existence of C═O group shows that part of glucose in the solution is converted into gluconic acid, and its reaction with magnesium accelerates the corrosion of pure Mg, which has been confirmed in our previous literature [55]. The deconvolution of N_{1s} spectra (Fig. 8(b)) reveals two components, centered at 399.5 eV and 400.3 eV, which correspond to the C–N and C═O–NH bonds, as expected for the amine or amide groups of BSA. As shown in Fig. 8(c), the binding energy of N_{1s} photoelectrons has three peaks at 397.3 eV, 396.7 eV and 398.2 eV, corresponding to O═C–NH, C–N and N–O/C–N, respectively. The results indicate that the adsorption of protein on the surface of pure magnesium. As shown in Fig. 8(e), the C_{1s} peaks on the sample in NaCl + BSA solution reveal three peaks related to the functions of C–C/C–H (284.6 eV), C–N/C–O (285.9 eV) and N–C═O (287.9 eV). These results are consistent with those of previous studies [60], indicating that the characteristic ions of amino acid can be tested. The existence of the albumin adsorbed on the sample surface plays a beneficial role by forming a barrier layer, which can prevent aggressive chlorine ions from penetrating from the electrolyte, thus decreasing the degradation rate of the magnesium substrate. Similar results can be observed from the narrow C_{1s} spectrum of the solution of NaCl + Glu + BSA, as shown in Fig. 8(f). The C_{1s} envelope shows four peaks associated with C–C/C–H (284.5 eV), C–N (285.4 eV), C═O (287.7 eV) and N–C═O (288.4 eV) groups. This finding indicates the presence of glucose compounds and protein compounds on the surface.

3.4. Fluorescent Labeling experiment

Fig. 9 reveals the fluorescence image of the adsorption of albumin (0.1 g/L) and glucose (2 g/L) on the surface of magnesium alloy at different immersion times by laser confocal microscopy. The green fluorescence images (Fig. 9a and c) are derived from fluorescein isothiocyanate-labeled albumin, and the red fluorescence images (Fig. 9b

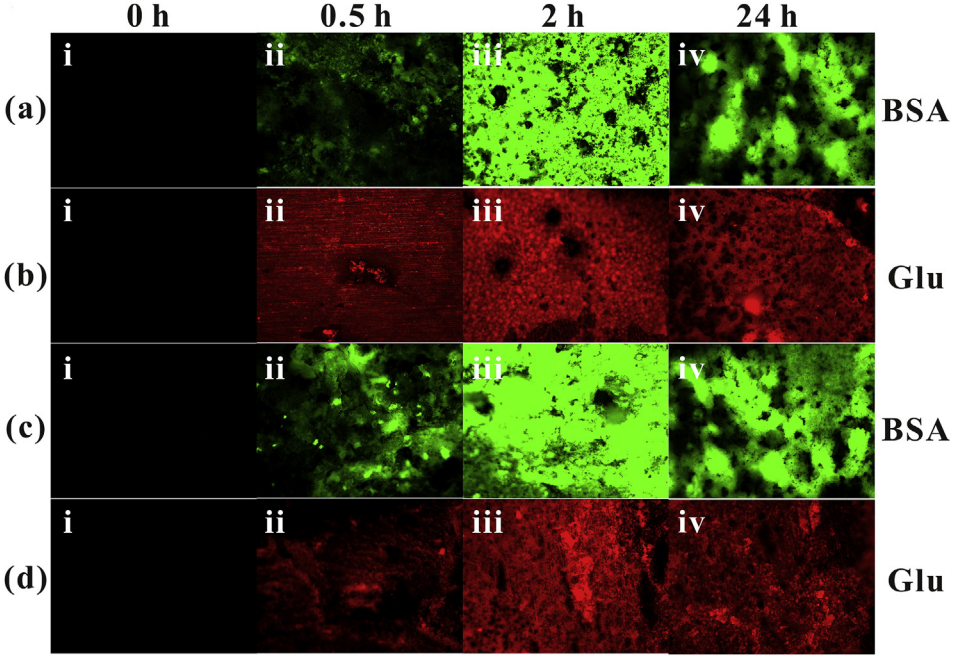

Fig. 9. Fluorescent Labeling spectra of the samples in: four solutions ((a)NaCl BSA,(b)NaCl Glu,(c)-(d)NaCl Glu + BSA) the samples in a 37 °C incubator after an immersion of (i) 0 h, (ii) 0.5 h, (iii) 2 h and (iv) 24 h.

and d) are derived from sodium fluorescein-labeled glucose [23,32]. It can be concluded from the figures that when the adsorption time of BSA on pure magnesium surface is 0.5 h, a small amount of protein is locally adsorbed on the surface of the sample, and the adsorption amount of protein on the magnesium surface increases with the prolong of adsorption time; when the adsorption time is extended from 0.5 h to 2 h The green fluorescent protein has almost completely covered the surface of the magnesium alloy and the brightness is increased, and the surface is partially defective. It is presumed that: the amount of protein adsorption increases, and the thickness of the film increases; the reason is that the magnesium substrate is corroded, the surface roughness is increased, and the protein adsorption is increased and the protein adsorption layer is not uniform. Continuing to extend the immersion time to 24 h, the green fluorescence covers the magnesium surface and the surface appears to be significantly depressed. The result is probably due to the chelation of protein and corrosion layer, which leads to the uneven corrosion of magnesium matrix and the shedding of some protein sites. The depression is likely to be the result of pitting corrosion. Fig. 9(c) shows a slight increase in protein adsorption compared with Fig. 9(a). It can be inferred that the presence of glucose promotes protein adsorption. This conjecture is consistent with the result of XPS.

4. Discussion

4.1. Influence of glucose content on degradation of pure Mg

In order to probe into the influence of glucose on the degradation behavior of pure magnesium in saline solution, we performed hydrogen evolution measurement and electrochemical test on samples immersed in saline solutions with different glucose concentrations (0 g/L, 2 g/L and 20 g/L). (Fig. 10). Our previous work has explored the effect of different glucose concentrations in saline solution on the degradation of magnesium alloys. The data (corrosion current density i_{corr} and corrosion rate) are summarized in Table 4. Zeng et al. [55] found that changes in glucose concentration may cause changes in the interface microenvironment of implanted metal materials in the human body. Glucose (25 g/L and 50 g/L) accelerated the degradation of pure magnesium in 0.9 wt % NaCl solution; however, the addition of glucose (1 g/L, 2 g/L, 3 g/L) in Hanks solution inhibited the corrosion of pure magnesium; Cui et al. [58] found that the adjunction of high concentration glucose promotes the degradation of Mg-1.35Ca alloy in saline solution. The electrochemical analysis of Li et al. [57] showed that the corrosion rate of magnesium alloy AZ31 is not affected by the low concentration of glucose. Wang et al. [56] concluded that glucose (2 g/L) may inhibit the degradation of pure magnesium. In the present study, we come to the same conclusion that the degradation of pure magnesium is inhibited by low concentration of glucose, and the corrosion rate is accelerated by high concentration of glucose (20 g/L).

As shown in Fig. 10(a) and (b), the hydrogen evolution rate (HER) curve shows a similar trend. In all cases, HER (the first 5 h) will increase rapidly and then gradually decrease until it reaches stability. This is due to pitting corrosion occurs after immersing the sample in the solution for several hours, and then HER falls owing to the formation of the corrosion product film and eventually reaches an equilibrium surface. Note that an increase in glucose content results in an apparent decrease in HER. In the initial soaking time, the HER in the saline solution with 2 g/L glucose was lower than the HER in saline with 20 g/L glucose. In the long soaking time (after 14 h), the HER in the saline solution with 2 g/L glucose was higher than the HER in saline with 20 g/L glucose.

The pH results show that the degradation process of the magnesium alloy in the saline solution is alkalized (as shown in Fig. 10(c)). This may be due to the different levels of conversion to gluconic acid resulting in different pH values.

As can be seen from Fig. 10(d–g), the addition of glucose (2 g/L) to physiological saline inhibited the corrosion of the sample in the saline solution, while the addition of glucose (20 g/L) accelerated the degradation of pure magnesium in the solution. The differences observed at different concentrations highlight the key effects on glucose content. Low concentration of glucose can change the microstructure of the surface of pure magnesium and inhibit its degradation. Glucose at high concentration can quickly convert into gluconic acid, and then react with the surface protective layer to promote the corrosion of pure magnesium. We still need to do further research to better understand these potential impacts.

A schematic diagram of the potential degradation mechanism of pure magnesium immersed in saline solution without glucose and with

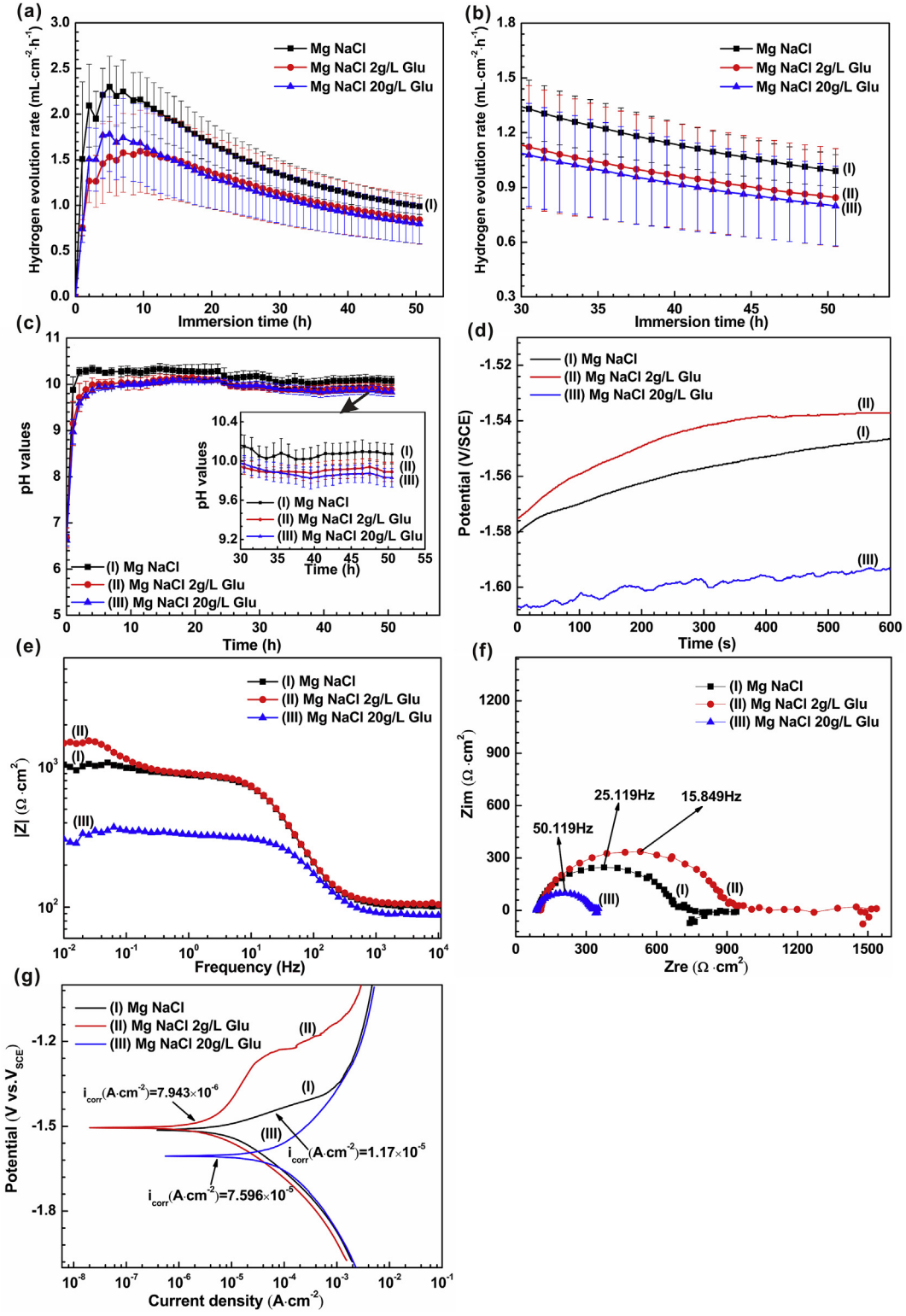

Fig. 10. The comparisons of results between 2 g/L and 20 g/L glucose showing (a),(b) HER; and (c) pH value. And the plots of (d) open circuit potential (OCP); (e) Bode; (f) Nyquist and (g) Potentiodynamic polarization curves of pure Mg immersed in 0.9 wt% NaCl Solution (with the addition of different levels of glucose).

glucose for 50 h is shown in Fig. 11(a) and (b), respectively. When the samples were immersed in solution (Fig. 8(a)), magnesium quickly dissolved to release a massive amount of Mg^{2+} ions, alkaline hydroxyl anions and hydrogen gas. And a partially protective $Mg(OH)_2$ film layer is formed on the sample surface. (Formula (1), (2), (3).

$$Mg(s) \rightarrow Mg^{2+}(aq) + 2e^- \quad (1)$$

$$2H_2O + 2e^- \rightarrow H_2(g)\uparrow + 2OH^-(aq) \quad (2)$$

$$Mg^{2+}(aq) + 2OH^-(aq) \rightarrow Mg(OH)_2(s) \quad (3)$$

In addition, the presence of CO_2 in the air also has an effect on the degradation behavior of the sample surface. The CO_2 dissolved in water may form CO_3^{2-} or HCO_3^-, and then react with Mg^{2+} in the solution to form $MgCO_3$ or $Mg_7(CO_3)_5(OH)_4{\cdot}nH_2O$ (as measured by XRD). The

Table 4
Comparison of positive or negative influence of glucose on corrosion rate in different solutions.

Materials	Solutions	i_{corr} (A/cm^2)	Corrosion rate	Refs.
Pure Mg	0.9 wt% NaCl	2.99×10^{-5}		Zeng[55]
	0.9 wt% NaCl + 1 g/L Glu	6.82×10^{-6}	↓	
	0.9 wt% NaCl + 2 g/L Glu	4.52×10^{-6}	↓	
	0.9 wt% NaCl + 3 g/L Glu	3.62×10^{-6}	↓	
	0.9 wt% NaCl + 25 g/L Glu	9.37×10^{-5}	↑	
	0.9 wt% NaCl + 50 g/L Glu	9.17×10^{-5}	↑	
Mg-1.35Ca	0.9 wt% NaCl	2.06×10^{-5}		Cui[58]
	0.9 wt% NaCl + 25 g/L Glu	3.2×10^{-5}	↑	
	0.9 wt% NaCl + 50 g/L Glu	4.03×10^{-5}	↑	
AZ31	0.9 wt% NaCl	2.76×10^{-5}		Li[57]
	0.9 wt% NaCl + 1 g/L Glu	1.51×10^{-5}	↓	
	0.9 wt% NaCl + 2 g/L Glu	2.47×10^{-5}	↓	
	0.9 wt% NaCl + 3 g/L Glu	2.91×10^{-5}	↑	
Pure Mg	0.9 wt% NaCl	6.9×10^{-6}		Wang[56]
	0.9 wt% NaCl + 2 g/L Glu	5.81×10^{-6}	↓	
	0.9 wt% NaCl + 25 g/L Glu	9.37×10^{-5}	↑	
Pure Mg	0.9 wt% NaCl	$(1.17 \pm 0.21) \times 10^{-5}$		Present work
	0.9 wt% NaCl + 2 g/L Glu	$(7.94 \pm 0.46) \times 10^{-6}$	↓	
	0.9 wt% NaCl + 20 g/L Glu	$(7.60 \pm 0.43) \times 10^{-5}$	↑	

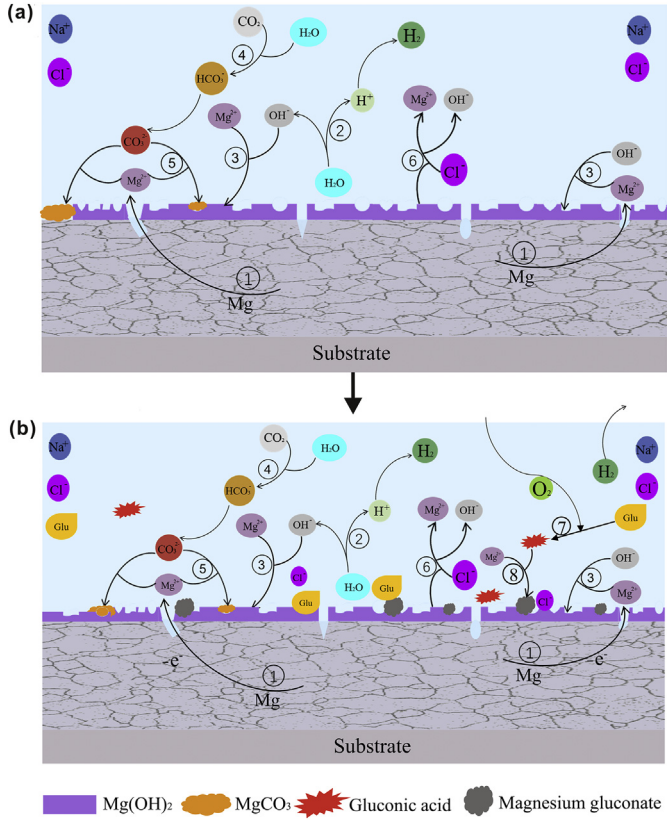

Fig. 11. Schematic illustration of the corrosion mechanism of pure Mg during immersion in:(a) solution NaCl and (b)solution NaCl Glu.

formation of a relatively thick layer of $MgCO_3$ can inhibit the erosion of chloride ions and contribute to the corrosion resistance of certain materials [47]. Some chemical reactions (Formulas (4), (5) are as follows [refs]:

$$CO_2 + H_2O \leftrightarrow H_2CO_3 \leftrightarrow HCO_3^- \quad (4)$$

$$7\,Mg(OH)_2 + 5\,HCO_3^- + (n\text{-}5)\,H_2O \rightarrow Mg_7(CO_3)_5(OH)_4{\cdot}nH_2O + 5OH^- \quad (5)$$

However, according to Formula (6), the $Mg(OH)_2$ film layer is susceptible to corrosion by corrosive chloride ions in solution and is converted to soluble $MgCl_2$. When the corrosion product dissolves and forms a dynamic equilibrium, the corrosion rate will gradually stabilize.

In our previous work, we explored the degradation behavior of glucose on pure magnesium. The results showed that the aldehyde group of glucose($(CH_2OH(CHOH)_4CHO)$) is active when glucose is added to physiological saline, and it is converted to gluconic acid ($CH_2OH(CHOH)_4COOH$) with an ionizing group (carboxyl group) under certain conditions (Formula (7)). Then, the glucose acid is capable of reacting with $Mg(OH)_2$ coating, slightly destroying the protective film, which is favorable for the precipitation of magnesium gluconate ($(CH_2OH(CHOH)_4COO)_2Mg$) on the sample surface (formula (8)). This hypothesis is a good explanation for the reduction in $Mg(OH)_2$ precipitation after the addition of glucose to the solution [55,58].

$$Cl^- + Mg(OH)_2 \rightarrow MgCl_2 + 2OH^- \quad (6)$$

$$CH_2OH(CHOH)_4CHO \rightarrow CH_2OH(CHOH)_4COOH\ (O_2, 37\ ^\circ C) \quad (7)$$

$$Mg^{2+} + 2CH_2OH(CHOH)_4COOH \rightarrow (CH_2OH(CHOH)_4COO)_2Mg + H_2\uparrow \quad (8)$$

We still need to do further research to gain a deeper comprehending of the mechanism of action of glucose on the degradation behavior of pure magnesium.

4.2. Influence of bovine serum albumin (BSA) on degradation

The previous studies on the effects of albumin on the degradation behavior of magnesium alloys have led to different conclusions. The data (corrosion current density i_{corr} and corrosion rate) are summarized in Table 5. Muller et al. [63] showed that the protein accelerates the corrosion rate of pure magnesium in PBS solution, and the degradation rate of magnesium alloy increases with the rise of protein concentration. They believed that the corrosion layer may be uneven and barely provide similar protection properties over the entire surface. Wang et al. [53] explored the effect of protein on the degradation behavior of M1A alloy in SBF solution. The results showed that the adsorption and chelation of proteins are manifested by inhibiting the corrosion of the MIA alloy in the initial stage and promoting the degradation of the alloy in the later stage. In addition, Fakiha et al. [75] studied the degradation behavior of different concentrations of bovine serum albumin (BSA) in simulated plasma. It is concluded that when the albumin concentration is 10–20 g/L, a complete adsorption protective layer can be formed on the alloy surface, which reduces the degradation rate of the magnesium alloy. While the concentration of BSA is lower than 10 g/L or higher than 20 g/L, the albumin can promote the corrosion of magnesium

Table 5
Comparison of positive or negative influence of protein on corrosion rate in different solutions.

Materials	Solutions	i_{corr} (A/cm^2)	Corrosion rate	Refs.
Pure Mg	PBS	$(7.76 \pm 8.81) \times 10^{-6}$		Mueller[63]
	PBS + 0.1 g/L BSA	$(3.53 \pm 3.39) \times 10^{-}$ [4]	↑	
	PBS + 1 g/L BSA	$(12.6 \pm 7.56) \times 10^{-}$ [5]	↑	
	PBS + 10 g/L BSA	$(3.73 \pm 5.41) \times 10^{-5}$	↑	
M1A	SBF	3.62×10^{-4}		Wang[53]
	SBF + 40 g/L BSA	2.81×10^{-4}	Frist ↓ Then ↑	
AZ80	SBP	2.82×10^{-6}		Fakiha[75]
	SBP + 5 g/L BSA	3.98×10^{-6}	↑	
	SBP + 10 g/L BSA	1.01×10^{-6}	↓	
	SBP + 20 g/L BSA	1.78×10^{-6}	↓	
	SBP + 40 g/L BSA	3.37×10^{-6}	↑	
Pure Mg	0.8 wt% NaCl	6.20×10^{-4}		Liu[69]
	0.8 wt% NaCl+1 g/L BSA	5.80×10^{-4}	↓	
	0.8 wt% NaCl+10 g/L BSA	4.50×10^{-4}	↓	
Pure Mg (PEO)	PBS	1.63×10^{-8}	–	Wan[60]
	PBS+1 g/L BSA	2.56×10^{-9}	↓	
	0.9 wt% NaCl	2.16×10^{-8}	–	
	0.9 wt% NaCl+1 g/L BSA	7.24×10^{-9}	↓	
Pure Mg	0.9 wt% NaCl	$(1.17 \pm 0.21) \times 10^{-5}$		Present work
	0.9 wt% NaCl+0.1 g/L BSA	$(3.97 \pm 0.53) \times 10^{-6}$	↓	
	0.9 wt% NaCl +10 g/L BSA	$(3.55 \pm 0.46) \times 10^{-5}$	↑	

alloy. Liu et al. [69] showed that in 0.8 wt% NaCl solution, albumin forms a protective membrane to inhibit the corrosion of pure Mg, and the higher the protein concentration, the better the protection ability. Wan et al. [60] obtained the same results that albumin had a certain inhibitory effect on the degradation behavior of pure magnesium in PBS solution and 0.9 wt% NaCl solution.

In order to better explore the effect of protein on the corrosion of pure Mg, we research the saline solution environment containing different concentration of albumin through hydrogen evolution measurement and electrochemical analysis. The results of hydrogen evolution experiment (Fig. 12(a-c)) showed that albumin could inhibit the degradation of pure Mg in saline solution. This is likely due to adsorption of negatively charged albumin molecules forming an integrated protective compact layer, which acts as a physical barrier to mitigate the alloy degradation [76]. Albumin molecules are composed of various amino acids linked by peptide bonds. Amino acid is composed of an amino group (-NH_2), a carboxyl group (-COOH), a central C and a side chain. The BSA has more acid amino acids than basic amino acids and Its isoelectric point is about 4.7 [52]. Owing to the pH value of the solution is higher than its isoelectric point, the protein is negatively charged in the brine solution. Therefore, albumin may bind to Mg^{2+} ions and adsorb on the sample surface to prevent further corrosion (formula (9)) [56].

$$Mg(OH)_2 + 2RCH(NH_2)COOH \rightarrow (RCH(NH_2)COO)_2Mg + 2H_2O \quad (9)$$

In other words, the micro amount of protein forms a thin layer through adsorption, which inhibits the degradation of magnesium in brine. However, the electrochemical analysis (Fig. 12(d-g)) show that low concentration (0.1 g/L) albumin inhibited the degradation of magnesium, while high concentration (10 g/L) albumin promoted the degradation of pure magnesium. The electrochemical results of high concentration albumin solution are different from those of hydrogen evolution. It has been accepted that the interaction between albumin and metal surface includes adsorption and chelation processes. When the chelation between BSA and metal ions exceeds the adsorption of BSA, it will stimulate the dissolution of metal. This indicates that the adsorption layer formed under the action of high concentration protein may be unstable.

4.3. Degradation mechanism of the synergetic effect of bovine serum Albumin(BSA) and glucose

Fig. 13 illustrates the potential corrosion mechanism of pure Mg in saline solution with protein and glucose. In the initial 2 h immersion (Figs. 1a and 13a), glucose and protein mainly promote the fast adsorption on the surface of pure magnesium to form a barrier layer on the surface of the sample and reduce the corrosion rate. When soaked for 2–10 h (Figs. 1(a) and 13(b)), the protein is negatively charged in the alkaline solution and will chelate with the positively charged Mg^{2+}, thus to a certain extent inhibiting the formation of the surface corrosion product magnesium hydroxide and accelerating the degradation rate of pure magnesium [32]. After immersion for 10 h (Fig. 13(c)), due to the consumption of protein and glucose in the later stage, the formation of the surface barrier layer and the erosion effect of chloride ion on the alloy surface are basically stable, and the corrosion rate tends to be gradually stable. From the results of XPS, we can see that the contents of C and N are obviously increased, which shows that glucose promotes the adsorption of protein on the sample surface to a certain extent.

Protein is a high molecular nitrogen-containing compound formed by peptide bond of amino acids. Some of its physical and chemical properties are similar to amino acids. When glucose and protein are present in the solution, the hemiacetal hydroxyl of glucose is replaced by the amino acid amino acid in protein, and a molecule of water is lost to form the amino acid glycosamine of glucose, which attributed to the Maillard reaction [77]. This is a nucleophilic substitution reaction and belongs to SN_2 mechanism. Previous studies have also shown that amino acids react with glucose in alkaline aqueous solutions [56,78]. The formula is as follows:

$$R_2C{=}O + R'NH_2 \rightarrow R_2C = NR' + H_2O \quad (10)$$

Amino acids and glucose have –NH_2 and –COH groups, respectively. When used in combination, the chemical reaction between $R_2C{=}O$ and $R'NH_2$ may be inevitable. The nitrogen atom of $R_2C = NR'$ group may be deprotonated in the alkaline solution, and then react with the positive Mg^{2+} ion, thus promoting the degradation rate of the alloy in the solution.

5. Conclusions

In this study, the effect of glucose and albumin on the corrosion behavior of pure Mg in physiological saline solution was investigated.

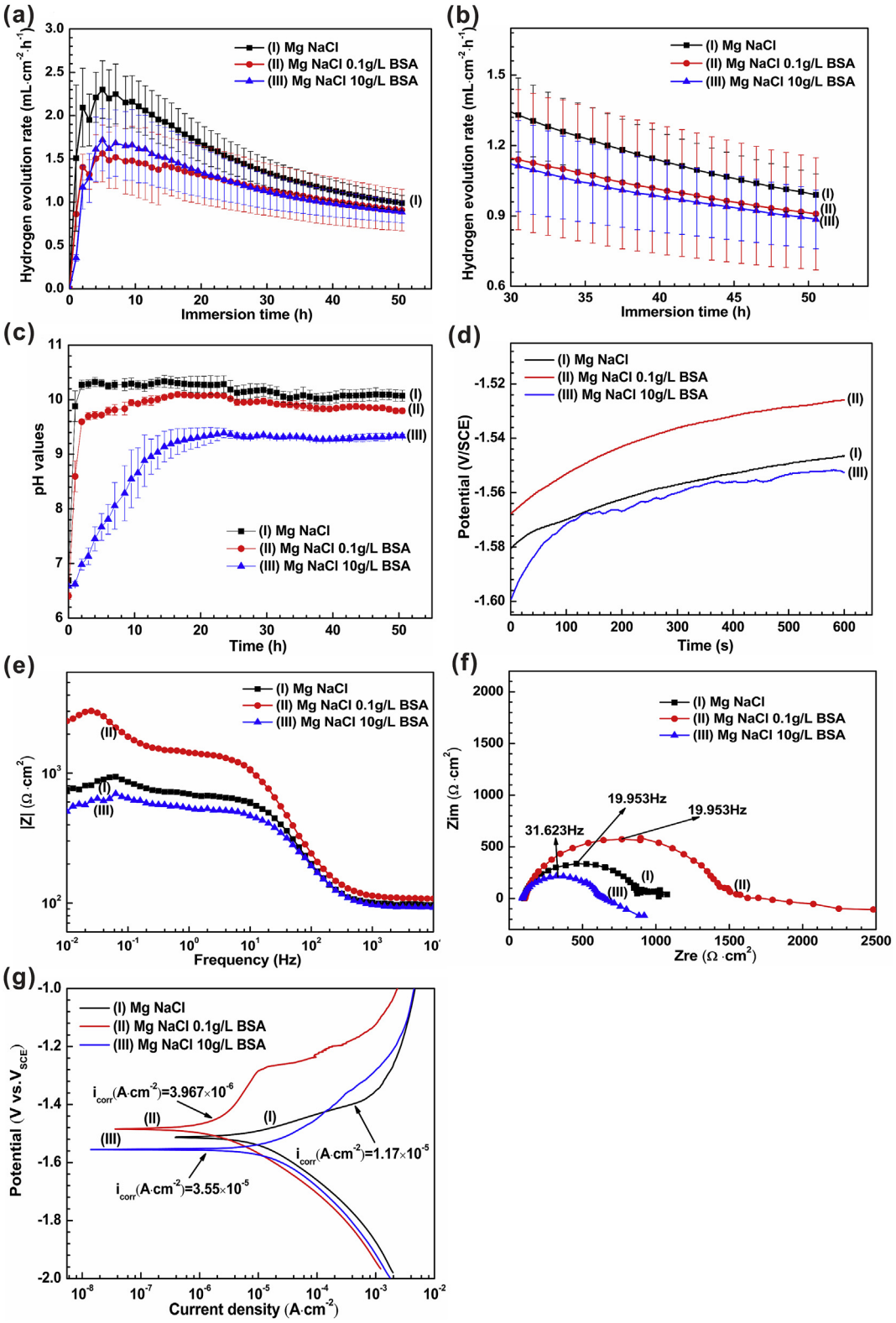

Fig. 12. Curves of (a)、(b) hydrogen evolution rate (HER) and (c) pH values as functions of immersion time. And the plots of (d) open circuit potential (OCP); (e) Bode; (f) Nyquist and (g) Potentiodynamic polarization curves of pure Mg immersed in 0.9 wt% NaCl Solution (with the addition of different levels of albumin).

The main results can be summarized as follows:

(1) Electrochemical tests showed that the existence of glucose (2 g/L) or BSA (0.1 g/L) decreased the degradation rate of pure Mg in 0.9 wt% NaCl. The hydrogen evolution test showed that the adsorption of albumin on sample at the early stage of immersion inhibited the degradation behavior, while the chelation of albumin with magnesium ions at the later stage promoted the corrosion of pure Mg in saline. The synergistic effect of glucose and albumin greatly inhibited the corrosion behavior of the sample.

(2) The results of fluorescence and XPS analysis showed that the adsorption and desorption of glucose and albumin on the sample

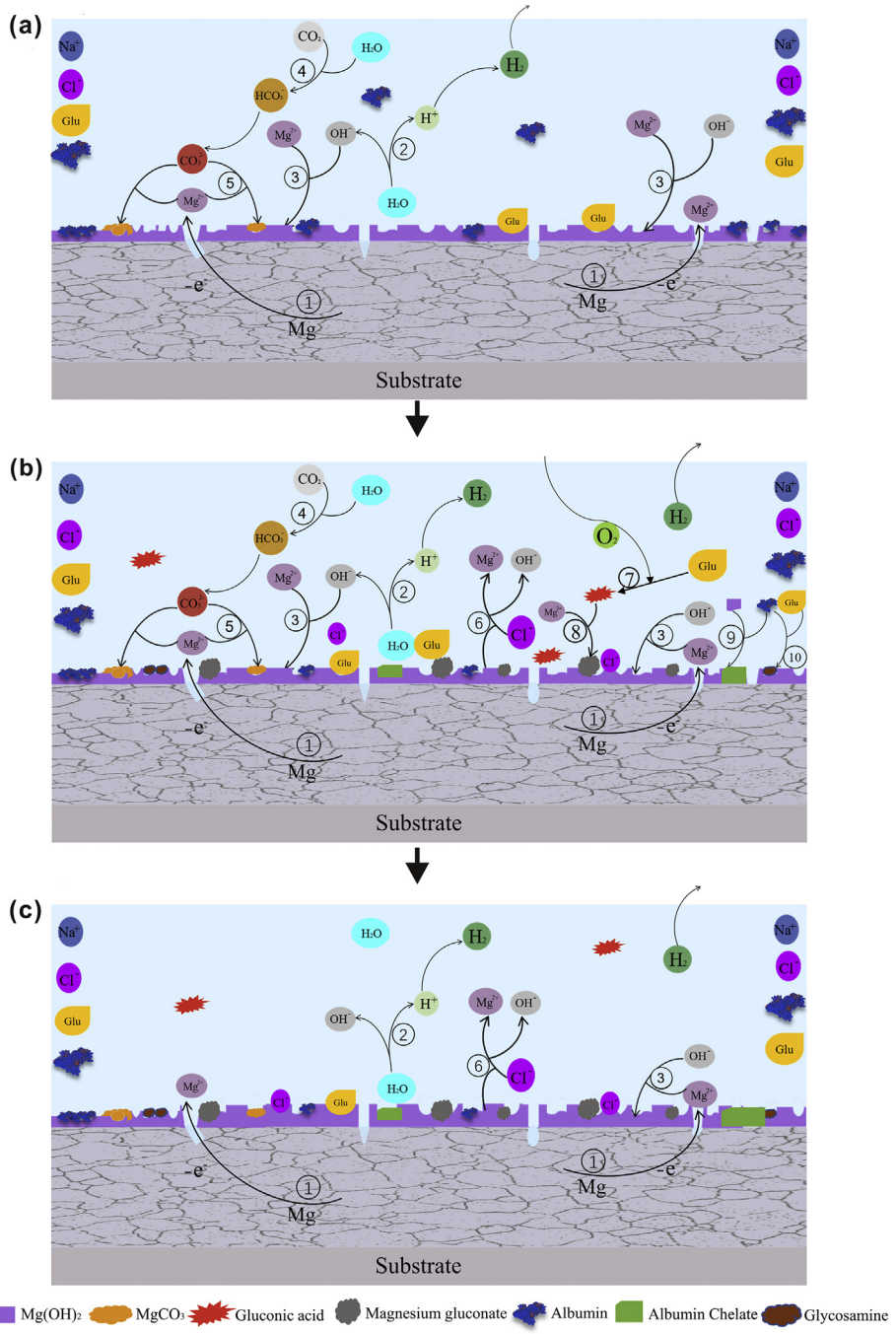

Fig. 13. Schematic illustration of the corrosion process of pure Mg during immersion in solution NaCl Glu + BSA: (a) stage i; (b) stage ii; and (c) stage iii.

surface. The increase of N element indicated that glucose promoted the adsorption of albumin.

(3) SEM, EDS and FTIR results showed that the corrosion product layer $Mg(OH)_2$ and the chelate of glucose (or albumin) with metal cations were formed on the surface.

(4) The results show that different concentrations of glucose (albumin) have different effects on the degradation of pure magnesium, and further study is needed to explore its mechanism.

CRediT authorship contribution statement

Wei Yan: Data curation, Writing - original draft. **Yi-Jie Lian:** Data curation. **Zhi-Yuan Zhang:** Data curation. **Mei-Qi Zeng:** Visualization, Investigation. **Zhao-Qi Zhang:** Software. **Zheng-Zheng Yin:** Software, Validation. **Lan-Yue Cui:** Conceptualization, Methodology. **Rong-Chang Zeng:** Visualization, Validation.

Declaration of competing interest

The authors declare that they have no known competing financial interests or personal relationships that could have appeared to influence the work reported in this paper.

Acknowledgments

This work was supported by the National Natural Science Foundation of China (51571134); the Scientific Research Foundation of Shandong University of Science and Technology Research Fund

(2014TDJH104) and Undergraduate Innovation and Entrepreneurship Training Program of Shandong University of Science and Technology (201710424082).

References

[1] G.L. Song, S.Z. Song, A possible biodegradable magnesium implant, Material Adv. Funct. Mater. 9 (2010) 298–302.

[2] L.Y. Qiao, J.C. Gao, Y. Wang, F.Y. Xie, Study of self-assembled monolayers of stearic acid on pure magnesium surface, Adv. Mater. Res. 415–417 (2012) 1279–1283.

[3] Y. Liu, Y.F. Zheng, X.H. Chen, J.A. Yang, H.B. Pan, D.F. Chen, L.N. Wang, J.L. Zhang, D.H. Zhu, S.L. Wu, K. Yeung, R.C. Zeng, Y. Han, S.K. Guan, Fundamental theory of biodegradable metals-definition, criteria, and design, Adv. Funct. Mater. 29 (2019) 1805402.

[4] A. Atrens, G.L. Song, M. Liu, Z. Shi, F. Cao, M.S. Dargusch, Review of recent developments in the field of magnesium corrosion, Adv. Eng. Mater. 17 (2015) 400–453.

[5] R.C. Zeng, W. Dietzel, F. Witte, N. Hort, C. Blawert, Progress and challenge for magnesium alloys as biomaterials, Adv. Eng. Mater. 10 (2010) B3–B14.

[6] S.N.H. Mohamad Rodzi, H. Zuhailawati, B.K. Dhindaw, Mechanical and degradation behaviour of biodegradable magnesium–zinc/hydroxyapatite composite with different powder mixing techniques, J. Magnesium Alloys 7 (2019) 566–576.

[7] H. Wu, Z. Shi, X.M. Zhang, A.M. Qasim, S. Xiao, F. Zhang, Z.Z. Wu, G.S. Wu, K.J. Ding, P.K. Chu, Achieving an acid resistant surface on magnesium alloy via bio-inspired design, Appl. Surf. Sci. 478 (2019) 150–161.

[8] D. Maradze, A. Capel, N. Martin, M.P. Lewis, Y.F. Zheng, Y. Liu, In vitro investigation of cellular effects of magnesium and magnesium-calcium alloy corrosion products on skeletal muscle regeneration, J. Mater. Sci. Technol. 35 (2019) 2503–2512.

[9] Y. Li, Y. Ding, K. Munir, J. Lin, M. Brandt, A. Atrens, Y. Xiao, J.R. Kanwar, C. Wen, Novel beta-Ti35Zr28Nb alloy scaffolds manufactured using selective laser melting for bone implant applications, Acta Biomater. 87 (2019) 273–284.

[10] F.Z. Yang Y-Xin, Y-Hao Liu, Y-Chen Hou, L-Guo Wang, Y-Fan Zhou, S-Jie Zhu, R-Chang Zeng, Y-Feng Zheng, S-Kang Guan, Biodegradation, hemocompatibility and covalent bonding mechanism of electrografting polyethylacrylate coating on Mg alloy for cardiovascular stent, J. Mater. Sci. Technol. (2020).

[11] S. Höhn, S. Virtanen, A.R. Boccaccini, Protein adsorption on magnesium and its alloys: a review, Appl. Surf. Sci. 464 (2019) 212–219.

[12] L.-Y. Cui, S.-C. Cheng, L.-X. Liang, J.-C. Zhang, S.-Q. Li, Z.-L. Wang, R.-C. Zeng, In vitro corrosion resistance of layer-by-layer assembled polyacrylic acid multilayers induced Ca–P coating on magnesium alloy AZ31, Bioact. Mater. 5 (2020) 153–163.

[13] P. Wan, L.L. Tan, K. Yang, Surface modification on biodegradable magnesium alloys as orthopedic implant materials to improve the bio-adaptability: a review, J. Mater. Sci. Technol. 32 (2016) 827–834.

[14] P. Amaravathy, T.S.S. Kumar, Bioactivity enhancement by Sr doped Zn-Ca-P coatings on biomedical magnesium alloy, J. Magnesium Alloys 7 (2019) 584–596.

[15] C.-Y. Li, C. Yu, R.-C. Zeng, B.-C. Zhang, L.-Y. Cui, J. Wan, Y. Xia, In vitro corrosion resistance of a Ta2O5 nanofilm on MAO coated magnesium alloy AZ31 by atomic layer deposition, Bioact. Mater. 5 (2020) 34–43.

[16] M.-S. Song, R.-C. Zeng, Y.-F. Ding, R.W. Li, M. Easton, I. Cole, N. Birbilis, X.-B. Chen, Recent advances in biodegradation controls over Mg alloys for bone fracture management: a review, J. Mater. Sci. Technol. 35 (2019) 535–544.

[17] Y.J. Zhang, C.W. Yan, F.H. Wang, W.F. Li, Electrochemical behavior of anodized Mg alloy AZ91D in chloride containing aqueous solution, Corros. Sci. 47 (2005) 2816–2831.

[18] L.C. Zhang, M.Z. Xu, Y.D. Hu, F. Gao, T. Gong, T. Liu, X. Li, C.J. Pan, Biofunctionization of biodegradable magnesium alloy to improve the in vitro corrosion resistance and biocompatibility, Appl. Surf. Sci. 451 (2018) 20–31.

[19] C. Ke, M.S. Song, R.C. Zeng, Y. Qiu, Y. Zhang, R.F. Zhang, R.L. Liu, I. Cole, N. Birbilis, X.B. Chen, Interfacial study of the formation mechanism of corrosion resistant strontium phosphate coatings upon Mg-3Al-4.3Ca-0.1Mn, Corros. Sci. 151 (2019) 143–153.

[20] Y.S. Feng, S.J. Zhu, L.G. Wang, L. Chang, B.B. Yan, X.Z. Song, S.K. Guan, Characterization and corrosion property of nano-rod-like HA on fluoride coating supported on Mg-Zn-Ca alloy, Bioact. Mater. 2 (2017) 63–70.

[21] Y.S. Feng, S.J. Zhu, L.G. Wang, L. Chang, Y.C. Hou, S.K. Guan, Fabrication and characterization of biodegradable Mg-Zn-Y-Nd-Ag alloy: microstructure, mechanical properties, corrosion behavior and antibacterial activities, Bioact. Mater. 3 (2018) 225–235.

[22] L. Chen, J.G. Li, S. Wang, S.J. Zhu, C. Zhu, B.Y. Zheng, G. Yang, S.K. Guan, Surface modification of the biodegradable cardiovascular stent material Mg–Zn–Y–Nd alloy via conjugating REDV peptide for better endothelialization, J. Mater. Res. 33 (2018) 4123–4133.

[23] L. Chen, J.A. Li, J.W. Chang, S.B. Jin, D. Wu, H.H. Yan, X.F. Wang, S.K. Guan, Mg-Zn-Y-Nd coated with citric acid and dopamine by layer-by-layer self-assembly to improve surface biocompatibility, Sci. China Technol. Sci. 61 (2018) 1228–1237.

[24] S. Johnston, C. Lau, M.S. Dargusch, A. Atrens, Absorbable Mg surgical tack: proof of concept &in situ fixation strength, J. Mech. Behav. Biomed. Mater. 97 (2019) 321–329.

[25] X. Ma, S.J. Zhu, L.G. Wang, C.X. Ji, C.X. Ren, S.K. Guan, Synthesis and properties of a bio-composite coating formed on magnesium alloy by one-step method of micro-arc oxidation, J. Alloys Compd. 590 (2014) 247–253.

[26] L.Y. Li, L.Y. Cui, R.C. Zeng, S.Q. Li, X.B. Chen, Y.F. Zheng, M.B. Kannan, Advances in functionalized polymer coatings on biodegradable magnesium alloys - A review, Acta Biomater. 79 (2018) 23–36.

[27] H. Wu, C. Zhang, T. Lou, B. Chen, R. Yi, W. Wang, R. Zhang, M. Zuo, H. Xu, P. Han, S. Zhang, J. Ni, X. Zhang, Crevice corrosion – a newly observed mechanism of degradation in biomedical magnesium, Acta Biomater. 98 (2019) 152–159.

[28] Z.-Z. Yin, W.-C. Qi, R.-C. Zeng, X.-B. Chen, C.-D. Gu, S.-K. Guan, Y.-F. Zheng, Advances in coatings on biodegradable magnesium alloys, J. Magnes. Alloys (2020).

[29] W. Wang, H. Wu, Y. Sun, J. Yan, L. Zhang, S. Zhang, J. Ni, Y. Song, X. Zhang, Local Intragranular Misorientation Accelerates Corrosion in Biodegradable Mg, Acta Biomater. (2019).

[30] Y. Song, S. Zhang, J. Li, C. Zhao, X. Zhang, Electrodeposition of Ca-P coatings on biodegradable Mg alloy: in vitro biomineralization behavior, Acta Biomater. 6 (2010) 1736–1742.

[31] S. Johnston, Z. Shi, J. Venezuela, C. Wen, M.S. Dargusch, A. Atrens, Investigating Mg biocorrosion in vitro: lessons learned and recommendations, J. Occup. Med. 71 (2019) 1406–1413.

[32] R.Q. Hou, R. Willumeit-Romer, V.M. Garamus, M. Frant, J. Koll, F. Feyerabenet, Adsorption of proteins on degradable magnesium-which factors are relevant? ACS Appl. Mater. Interfaces 10 (2018) 42175–42185.

[33] C.L. Liu, Y.J. Wang, R.C. Zeng, X.M. Zhang, W.J. Huang, P.K. Chu, In vitro corrosion degradation behaviour of Mg–Ca alloy in the presence of albumin, Corros. Sci. 52 (2010) 3341–3347.

[34] B. Ratna Sunil, T.S. Sampath Kumar, U. Chakkingal, V. Nandakumar, M. Doble, V. Devi Prasad, M. Raghunath, In vitro and in vivo studies of biodegradable fine grained AZ31 magnesium alloy produced by equal channel angular pressing, Mater. Sci. Eng. C 59 (2016) 356–367.

[35] J. Walker, S. Shadanbaz, N.T. Kirkland, E. Stace, T. Woodfield, M.P. Staiger, G.J. Dias, Magnesium alloys: predicting in vivo corrosion with in vitro immersion testing, J. Biomed. Mater. Res. B Appl. Biomater. 100 (2012) 1134–1141.

[36] F. Witte, J. Fischer, J. Nellesen, H.-A. Crostack, V. Kaese, A. Pisch, F. Beckmann, H. Windhagen, In vitro and in vivo corrosion measurements of magnesium alloys, Biomaterials 27 (2006) 1013–1018.

[37] S. Zhang, X. Zhang, C. Zhao, J. Li, Y. Song, C. Xie, H. Tao, Y. Zhang, Y. He, Y. Jiang, Y. Bian, Research on an Mg–Zn alloy as a degradable biomaterial, Acta Biomater. 6 (2010) 626–640.

[38] S.X. Zhang, X.N. Zhang, C.L. Zhao, J.A. Li, Y. Song, C.Y. Xie, H.R. Tao, Y. Zhang, Y.H. He, Y. Jiang, Y.J. Bian, Research on an Mg-Zn alloy as a degradable biomaterial, Acta Biomater. 6 (2010) 626–640.

[39] A. Atrens, S. Johnston, Z. Shi, M.S. Dargusch, Viewpoint - understanding Mg corrosion in the body for biodegradable medical implants, Scripta Mater. 154 (2018) 92–100.

[40] P. Saha, M. Roy, M.K. Datta, B. Lee, P.N. Kumta, Effects of grain refinement on the biocorrosion and in vitro bioactivity of magnesium, Mater. Sci. Eng.: Chimia 57 (2015) 294–303.

[41] R.C. Zeng, L.Y. Cui, W. Ke, Biomedical magnesium alloys: composition, microstructure and corrosion, Acta Metall. Sinica 54 (2018) 1215–1235 Chinese Edition.

[42] X. Liu, J.L. Xue, D. Zhang, Electrochemical behaviors and discharge performance of the as-extruded Mg-1.5 wt%Ca alloys as anode for Mg-air battery, J. Alloys Compd. 790 (2019) 822–828.

[43] A. Yamamoto, S. Hiromoto, Effect of inorganic salts, amino acids and proteins on the degradation of pure magnesium in vitro, Mater. Sci. Eng. C 29 (2009) 1559–1568.

[44] Y.F. Zhang, F. Feyerabend, S.W. Tang, J. Hu, X.P. Lu, C. Blawert, T.G. Lin, A study of degradation resistance and cytocompatibility of super-hydrophobic coating on magnesium, Mater. Sci. Eng.: Chimia 78 (2017) 405–412.

[45] G. Song, A. Atrens, D.S. John, X. Wu, J. Nairn, The anodic dissolution of magnesium in chloride and sulphate solutions, Corros. Sci. 39 (1997) 1981–2004.

[46] Y.C. Xin, K.F. Huo, H. Tao, G.Y. Tang, P.K. Chu, Influence of aggressive ions on the degradation behavior of biomedical magnesium alloy in physiological environment, Acta Biomater. 4 (2008) 2008–2015.

[47] R.C. Zeng, Y. Hu, S.K. Guan, H.Z. Cui, E.H. Han, Corrosion of magnesium alloy AZ31: the influence of bicarbonate, sulphate, hydrogen phosphate and dihydrogen phosphate ions in saline solution, Corros. Sci. 86 (2014) 171–182.

[48] Z. Fang, J.F. Wang, X.F. Yang, Q. Sun, Y. Jia, H.R. Liu, T.F. Xi, S.K. Guan, Adsorption of arginine, glycine and aspartic acid on Mg and Mg-based alloy surfaces: a first-principles study, Appl. Surf. Sci. 409 (2017) 149–155.

[49] Z. Fang, J.F. Wang, S.J. Zhu, X.F. Yang, S.K. Guan, A DFT study of the adsorption of short peptides on Mg and Mg-based alloy surfaces, Phys. Chem. Chem. Phys. 20 (2018) 3602–3607.

[50] J. Kim, Mathematical modeling approaches to describe the dynamics of protein adsorption at solid interfaces, Colloids Surf., B 162 (2018) 370–379.

[51] B. Neirinck, F. Singer, A. Braem, S. Virtanen, J. Vleugels, Alternating current electrophoretic deposition of bovine serum albumin onto magnesium key, Eng. Mater. 654 (2015) 139–143.

[52] L. Rui, Z. Wu, Y. Wangb, L. Ding, Y. Wang, Role of pH-induced structural change in protein aggregation in foam fractionation of bovine serum albumin, Biotechnol. Rep. 9 (2016) 46–52.

[53] Y.S. Wang, S.L. Chu, V.L. Chao, S.Y. Ming, E.K. Teo, L.N. Moh, In vitro degradation behavior of M1A magnesium alloy in protein-containing simulated body fluid, Mater. Sci. Eng. C 31 (2011) 579–587.

[54] P. Liu, J.-M. Wang, X.-T. Yu, X.-B. Chen, S.-Q. Li, D.-C. Chen, S.-K. Guan, R.-C. Zeng, L.-Y. Cui, Corrosion resistance of bioinspired DNA-induced Ca–P coating on biodegradable magnesium alloy, J. Mag. Alloys 7 (2019) 144–154.

[55] R.C. Zeng, X.T. Li, S.Q. Li, F. Zhang, E.H. Han, In vitro degradation of pure Mg in response to glucose, Sci. Rep. 5 (2015) 13026.

[56] Y. Wang, L.Y. Cui, R.C. Zeng, S.Q. Li, Y.H. Zou, E.H. Han, In vitro degradation of

pure magnesium-the effects of glucose and/or amino acid, Materials 10 (2017) 725.
[57] L.Y. Li, B. Liu, R.C. Zeng, S.Q. Li, Q.Y. Liu, In vitro corrosion of magnesium alloy AZ31 — a synergetic influence of glucose and Tris, Front. Mater. Sci. 12 (2018) 184–197.
[58] L.Y. Cui, X.T. Li, R.C. Zeng, S.Q. Li, E.H. Han, L. Song, In vitro corrosion of Mg–Ca alloy — the influence of glucose content, Front. Mater. Sci. 11 (2017) 284–295.
[59] D. Hwang, and H.-L. Wang Medical Contraindications to Implant Therapy: Part II: Relative Contraindications Implant Dentistry, vol 16, pp. 13-23.
[60] P. Wan, X. Lin, L.L. Tan, L. Li, W.R. Li, K. Yang, Influence of albumin and inorganic ions on electrochemical corrosion behavior of plasma electrolytic oxidation coated magnesium for surgical implants, Appl. Surf. Sci. 282 (2013) 186–194.
[61] C.L. Liu, Y.C. Xin, X.B. Tian, P.K. Chu, Degradation susceptibility of surgical magnesium alloy in artificial biological fluid containing albumin, J. Mater. Res. 22 (2007) 1806–1814.
[62] R. Rettig, S. Virtanen, Composition of corrosion layers on a magnesium rare-earth alloy in simulated body fluids, J. Biomed. Mater. Res. 88A (2009) 359–369.
[63] W.D. Mueller, M.F. de Mele, M.L. Nascimento, M. Zeddies, Degradation of magnesium and its alloys: dependence on the composition of the synthetic biological media, J. Biomed. Mater. Res. 90A (2010) 487–495.
[64] Y. Wang, B.H. Ding, S.Y. Gao, X.B. Chen, R.C. Zeng, L.Y. Cui, S.J. Li, S.Q. Li, Y.H. Zou, E.H. Han, S.K. Guan, Q.Y. Liu, In vitro corrosion of pure Mg in phosphate buffer solution-Influences of isoelectric point and molecular structure of amino acids, Mater. Sci. Eng. C Mater. Biol. Appl. 105 (2019) 110042.
[65] E. Balint, P. Szabo, C.F. Marshall, S.M. Sprague, Glucose-induced inhibition of in vitro bone mineralization, Bone 28 (2001) 21–28.
[66] Z.Q. Zhang, R.C. Zeng, C.G. Lin, L. Wang, X.B. Chen, D.C. Chen, Corrosion resistance of self-cleaning silane/polypropylene composite coatings on magnesium alloy AZ31, J. Mater. Sci. Technol. 41 (2020) 43–55.
[67] L.Y. Cui, H.P. Liu, W.L. Zhang, Z.Z. Han, M.X. Deng, R.C. Zeng, S.Q. Li, Z.L. Wang, Corrosion resistance of a superhydrophobic micro-arc oxidation coating on Mg-4Li-1Ca alloy, J. Mater. Sci. Technol. 33 (2017) 1263–1271.
[68] L.J. Liu, Y. Meng, A.A. Volinsky, H.J. Zhang, L.N. Wang, Influences of albumin on in vitro corrosion of pure Zn in artificial plasma, Corrosion Sci. 153 (2019) 341–356.
[69] C.L. Liu, Y. Zhang, C.Y. Zhang, W. Wang, W.J. Huang, P.K. Chu, Synergistic effect of chloride ion and albumin on the corrosion of pure magnesium, Front. Mater. Sci. China 8 (2014) 244–255.
[70] F. Zhang, C.L. Zhang, R.C. Zeng, L. Song, L. Guo, X.W. Huang, Corrosion Resistance of the Superhydrophobic Mg(OH)2/Mg-Al Layered Double Hydroxide Coatings on Magnesium Alloys Metals vol 6, (2016).
[71] I. Johnson, W.S. Jiang, H.N. Liu, The effects of serum proteins on magnesium alloy degradation in vitro, Sci. Rep. 7 (2017).
[72] A. Carangelo, A. Acquesta, T. Monetta, In-vitro corrosion of AZ31 magnesium alloys by using a polydopamine coating, Bioact. Mater. 4 (2019) 71–78.
[73] J.E. Gray-Munro, M. Strong, A study on the interfacial chemistry of magnesium hydroxide surfaces in aqueous phosphate solutions: influence of Ca2+, Cl− and protein, J. Colloid Interface Sci. 393 (2013) 421–428.
[74] L.Y. Cui, X.H. Fang, W. Cao, R.C. Zeng, S.Q. Li, X.B. Chen, Y.H. Zou, S.K. Guan, E.H. Han, In vitro corrosion resistance of a layer-by-layer assembled DNA coating on magnesium alloy, Appl. Surf. Sci. 457 (2018) 49–58.
[75] F.E.T. Heakal, A.M. Bakry, Serum albumin can influence magnesium alloy degradation in simulated blood plasma for cardiovascular stenting, Mater. Chem. Phys. 220 (2018) 35–49.
[76] Z. Fang, Y. Zhao, H. Wang, J. Wang, S. Zhu, Y. Jia, J.-H. Cho, S. Guan, Influence of surface charge density on ligand-metal bonding: a DFT study of NH3 and HCOOH on Mg (0 0 0 1) surface, Appl. Surf. Sci. 470 (2019) 893–898.
[77] W.H. Zheng, X. Xu, Research Progress on Maillard Reaction Progress in Chemistry, 17 (2005), pp. 122–129.
[78] S. Lin, M. Zhang, J. Liu, G.S. Jones, Construction and application of recombinant strain for the production of an alkaline protease from Bacillus licheniformis, J. Biosci. Bioeng. 119 (2015) 284–288.